Coronary constriction impairs cardiac function and induces myocardial damage and ventricular remodeling in mice

BAOSHENG LI, QIONG LI, XIAOWEI WANG, KUMAR P. JANA,
GIORGIO REDAELLI, JAN KAJSTURA, AND PIERO ANVERSA
Department of Medicine, New York Medical College, Valhalla, New York 10595

Li, Baosheng, Qiong Li, Xiaowei Wang, Kumar P. Jana, Giorgio Redaelli, Jan Kajstura, and Piero Anversa. Coronary constriction impairs cardiac function and induces myocardial damage and ventricular remodeling in mice. *Am. J. Physiol.* 273 (*Heart Circ. Physiol.* 42): H2508–H2519, 1997.—To establish whether coronary artery narrowing (CAN) in mice was accompanied by depressed ventricular function, tissue injury, and modifications in cardiac anatomy, the left coronary artery was constricted in FVB/N mice and the animals were killed 7 days later. CAN consisted of a 53% reduction in luminal diameter, which resulted in a twofold increase in left ventricular end-diastolic pressure. Left ventricular systolic pressure and left ventricular + and −dP/d*t* decreased 15, 21, and 11%, respectively. Left ventricular weight-to-body weight ratio increased 33%. This hypertrophic adaptation was characterized by a 9 and 20% increase in the longitudinal and transverse cavitary diameters, which provoked a 1.5-fold expansion in chamber volume. In contrast, wall thickness decreased 15%. These anatomic and functional changes induced a threefold elevation in diastolic stress. Foci of reparative fibrosis were found in the endomyocardium and epimyocardium, involving 2–3% of the tissue. Finally, myocyte loss in the ventricle was 15%, and myocyte hypertrophy was 38%. Impaired ventricular function, diastolic Laplace overloading, myocyte loss, and decompensated eccentric hypertrophy in mice after CAN mimic the ischemic cardiomyopathic heart in humans.

coronary artery stenosis; ventricular dysfunction; myocyte number; replacement fibrosis; decompensated eccentric hypertrophy

ISCHEMIC CARDIOMYOPATHY is characterized by an imbalance between oxygen supply and demand that alters the structure and function of the heart (1, 2). The clinical syndrome is created by partial or complete occlusion of a major epicardial coronary artery that results in multiple focal sites of tissue injury across the wall or a segmental involvement of the ventricle, reflecting a myocardial infarct (7, 30). Recent observations in animal models, mimicking the human disease, have raised the possibility that coronary artery constriction and scattered myocyte loss have a detrimental impact on ventricular performance that exceeds the influence of myocardial infarction (2). In this regard, acute transient ischemic episodes have profound consequences on ventricular size and shape (32), and sudden decreases in coronary blood flow of 10–20% impair regional cardiac function (28). Moreover, changes in myocardial perfusion with coronary artery stenosis do not correlate with the reductions in luminal diameter (9), suggesting that other factors systemically and/or locally may be implicated in the ischemic myopathy. Similarly, in patients affected by chronic coronary artery disease, the degree of constriction does not correspond to the severity of the clinical manifestations of cardiac dysfunction and failure (31). Conversely, the magnitude of structural damage seems to be coupled with the depression in ventricular hemodynamics in both humans and animals (2, 23), although a cause-and-effect relationship between cell death and impairment in cardiac function remains to be determined.

These unresolved issues have prompted us to develop a mouse model of coronary artery narrowing (CAN), because molecular interventions enhancing the coronary vasculature (3) or interfering with cell death (29) and cell growth (24) and eventually wall and chamber remodeling will be more commonly introduced and analyzed in this species. In addition, mutation and deletion of genes implicated in myocyte mechanics are almost exclusively performed in mice (17). The objective here was to document whether the surgical imposition of CAN was possible in mice and whether this procedure was capable of inducing tissue injury, alterations in cavitary volume and mural thickness, and abnormalities in pump function and myocardial loading. A 7-day time interval was selected to establish whether myocardial damage was present and contributed to the restructuring of the ventricle and its performance, creating a condition typically observed in the cardiomyopathic heart of ischemic origin in humans.

MATERIAL AND METHODS

Coronary artery constriction. Experiments were carried out in male FVB/N mice at 75 days of age (Taconic Farms, Germantown, NY). With mice under ether anesthesia and with the aid of an operating microscope (Zeiss-Urban Quadrascope, Zeiss, Germany), thoracotomy via the third left intercostal space was performed, the atrial appendage was elevated, the left coronary artery was located, and a silk black braided suture (6–0) was inserted around the vessel near its origin. The left coronary artery is positioned between the left atrial appendage and the pulmonary artery, beneath the pericardium, and within the epicardial muscle layer. The vessel was not dissected free and a needle was used to pass the suture under the vessel. This approach was preferred because preliminary attempts with dissection of the vessel resulted in rupture of the coronary artery and hemorrhage. A probe of 140 μm in diameter was held in contact with the myocardium over the vessel and between the entrance and exit of the suture. The entire vessel and the probe were ligated, and the probe was quickly removed (2, 9). The chest was closed, the pneumothorax was reduced by negative pressure, and the mice were allowed to recover. To reduce postoperative pain, buprenorphine hydrochloride (0.65 mg/kg body wt) was injected intramuscularly (Buprenex; Reckitt and Colman Pharmaceuticals, Richmond, VA). This dose corresponds to 5 mg/kg body wt of morphine sulfate. The

administration of this drug was repeated 6–8 and 12–16 h later. Sham-operated control mice were treated similarly, except that the ligature around the coronary artery was not tied. Animals were not mechanically ventilated because the entire operation, between the opening of the thorax and the completion of surgery, did not last >30 s. Additionally, chloral hydrate, a longer-duration anesthetic, was associated with increased immediate postoperative mortality. During the procedure, it was inevitable to include in the ligature some muscle mass with distortion of the shape of the lumen. Because of the difficulty in reducing the diameter of a major coronary artery to a given degree with an external device, the actual level of constriction was measured at death. Coronary artery stenosis was successfully performed in 18 animals. Sixteen sham-operated mice served as controls. After chloral hydrate anesthesia, all animals were killed 7 days after surgery by arresting the heart in diastole with cadmium chloride (see *Fixation procedure*). Complications of the procedure and the rate of mortality are described in RESULTS.

Functional measurements. Just before death, animals were anesthetized with chloral hydrate (400 mg/kg body wt ip) and the external right carotid artery was exposed and cannulated with a microtip pressure transducer catheter (model SPR-612, Millar Instruments, Houston, TX) connected to an electrostatic chart recorder (model ES 2000, Gould, Cleveland, OH). This catheter was developed for mice and has a size of 1.8 F (0.71 mm), which is significantly smaller than chamber diameter. After arterial blood pressure was monitored, the catheter was advanced into the left ventricle for the evaluation of left ventricular pressures and the rate of rise in pressure (dP/d*t*). Thus measurements were made of systolic, diastolic, and mean arterial blood pressures and left ventricular pressures and dP/d*t* in the closed chest preparation. Rectal temperature, which varied between 36 and 38°C, was maintained during these determinations with the aid of a table lamp. The collection of these functional parameters carried some mortality, which is is indicated in RESULTS. This portion of the study included 16 sham-operated and 12 CAN mice. The experimental protocol employed for coronary artery constriction and for the evaluation of functional parameters was approved by the animal care committee of New York Medical College.

Fixation procedure. At the completion of the hemodynamic measurements, with the animals under chloral hydrate anesthesia, the abdominal aorta was cannulated with a polyethylene catheter (PE-50) and filled with phosphate buffer (0.2 M, pH 7.4) and heparin (100 IU/ml). In rapid succession, the heart was arrested in diastole by the injection of 0.15 ml of cadmium chloride (100 mM) through the aortic catheter, the thorax opened, perfusion with phosphate buffer started, and the right atrium cut to allow the drainage of blood and perfusate. The aortic catheter was connected to a pressure reservoir; perfusion pressure was adjusted to mean arterial pressure measured in vivo. Simultaneously, the left ventricular chamber was filled with fixative from a pressure reservoir set at a height equivalent to the in vivo measured end-diastolic pressure throughout the fixation procedure. This was accomplished by inserting a 25G3/4 Vacutainer (Becton Dickinson, Rutherford, NJ) into the left ventricle through the apex. The needle was also connected to the pressure reservoir (2). After perfusion with buffer for 2 min, the coronary vasculature was perfused for 15 min with 4% formaldehyde in phosphate buffer. Subsequently, the heart was excised, and the weights of the left ventricle, including the septum and the right ventricle, were recorded. The volume of left ventricular myocardium was then determined by dividing its weight by the specific gravity of muscle tissue, 1.06 g/ml (2). This part of the study included 16 sham-operated and 18 CAN mice.

Coronary artery diameter. The initial 0.5- to 1.0-mm segment of the left coronary artery was dissected free to localize the level of coronary constriction. The vessel was then cut transversely to expose the lumen of the coronary artery at the region of the ligature. The thickness of the suture was 150 μm. The luminal diameters of the vessel adjacent to the narrowed site and in the constricted portion were measured with a dissecting microscope with an incorporated ocular reticle. Maximal and minimal internal diameters were determined ×40, and the geometric mean value was calculated (2). The average luminal cross-sectional area was computed using these measurements. The degree of constriction was evaluated by comparing the vessel diameter above the stenosis with the diameter at the level of the stenosis. This approach was preferred to comparisons between experimental and sham-operated control mice to estimate the degree of constriction in the same vessel and minimize the variability in the coronary vasculature among animals. This analysis involved 16 sham-operated and 18 CAN mice.

Ventricular dimensions. The major intracavitary axis of the left ventricle from apex to base was measured first. Subsequently, the left ventricle was sectioned perpendicularly to the longitudinal axis to obtain a transverse section, 1.5 mm in thickness, halfway between the base and the apex in which the average wall thickness of the free wall and septum and chamber luminal diameter were measured. Minimal and maximal diameters of the ventricular chamber were determined, and their geometric mean was computed (2). The long and transverse diameters were employed to calculate chamber volume (1, 2). This analysis involved 16 sham-operated and 18 CAN mice. Moreover, the measurements of wall thickness, chamber radius, and ventricular end-diastolic pressure in the left ventricle were used to compute mid-wall circumferential diastolic stress (2). For this latter determination, *n* values were 16 sham-operated and 12 CAN mice.

Myocardial damage. Three slices of each left ventricle, from the basal, middle, and apical portions, were embedded in paraffin and sections, 4 μm in thickness, were obtained. These sections, which contained the entire thickness of the left ventricular wall and septum, were stained with hematoxylin and eosin or trichrome for quantitative measurements. The thickness of the left ventricular free wall was subdivided in two equal parts, and 60 consecutive fields, 30 each from the endomyocardium and epimyocardium in each heart, were examined at a calibrated magnification of ×400 with a reticle containing 42 sampling points (2). This reticle defined an uncompressed tissue area of 39,205 μm^2, which was used to determine the number of lesions represented by foci of damage per unit area of myocardium. The fraction of points lying over these foci was measured to compute the volume fraction of lesions in the tissue and the cross-sectional area of the lesion profiles. The septum was analyzed in terms of percent of tissue damage only. These determinations included 9 sham-operated and 10 CAN mice.

Myocyte size and number. Morphometric sampling at a magnification of ×1,000 consisted of counting the number of myocyte nuclear profiles [$N(n)$] in a measured area (A) of tissue sections in which cardiac muscle fibers were cut transversely. A square tissue area of 6,084 μm^2 was delineated in the microscopic field by the 42-sampling point ocular reticle. A total of 15 such fields each was evaluated in the endomyocardial and epimyocardial regions of each ventricle of each animal to determine the number of nuclear profiles per unit area of myocardium [$N(n)_A$] and the volume fraction of myocytes [$V(m)_V$] in the myocardium. Nuclear length [$\overline{D}(n)$] was determined in each left ventricle from 40 measurements made at ×1,250 in longitudinally oriented myocytes viewed

with a microscope with an ocular micrometer accurate to 0.5 μm.

From the estimation of $N(n)_A$ and $\overline{D}(n)$, the number of myocyte nuclei per unit volume of myocardium $[N(n)_V]$ was computed using the equation (2)

$$N(n)_V = N(n)_A/\overline{D}(n) \quad (1)$$

Myocyte cell volume per nucleus in each left ventricle $[\overline{V}(m)_n]$ was obtained from the volume fraction of myocytes $[V(m)_V]$ divided by the number of myocyte nuclei per unit volume of myocardium

$$\overline{V}(m)_n = V(m)_V/N(n)_V \quad (2)$$

The total number of ventricular myocyte nuclei $[N(n)_T]$ was derived from the product of $N(n)_V$ and the aggregate volume of viable myocardium in the ventricle $[V_T]$

$$N(n)_T = N(n)_V \times V_T \quad (3)$$

This analysis included 9 sham-operated and 10 CAN mice.

Data collection and analysis. Results are presented as means ± SD. Statistical significance for comparisons between two measurements was determined with the unpaired two-tailed Student's *t*-test. Morphometric data were collected blindly, and the code was broken at the end of the experiment. Because measurements presented were not obtained in all animals, *n* values for each parameter are listed in the text or in the legend to Figs. 1–9. In all cases, *n* values correspond to number of animals.

RESULTS

Cross-cardiac characteristics. Body weight in sham-operated mice, 26 ± 3 g ($n = 16$), was 8% larger than in mice subjected to CAN, 24 ± 4 g ($n = 18$), but this difference was not statistically significant. However, coronary constriction for 7 days resulted in a 22 ($P < 0.001$) and 19% ($P < 0.05$) increase in the weight of the left and right ventricle, respectively (Fig. 1*A*). These changes produced a 21% increase in total heart weight that was statistically significant ($P < 0.001$). Because of the decrease in body weight after CAN, the increases in cardiac weights with respect to body weight were greater than those detected with weight changes alone. A 32 ($P < 0.001$), 33 ($P < 0.001$), and 29% ($P < 0.01$) increase in heart and left and right ventricular weight-to body weight ratios were found with CAN (Fig. 1*B*). In summary, CAN at 7 days was characterized by left and right ventricular hypertrophy.

Coronary artery constriction. The surgical procedure used for stenosis of the left main coronary artery resulted in different reductions in luminal diameter, ranging from 36 to 80%. This variability reflected the 18 cases included in the study. However, 24 additional hearts were excluded from the analysis because 6 had myocardial infarction and 18 had minimal levels of narrowing and could not be used as controls. The induction of CAN in mice had a high degree of mortality. This was related in part to the difficulty of surgery and to the generation of large infarcts incompatible with life. Additionally, a number of animals died in the first 2–3 days after the operation. Overall mortality involved nearly 60% of the animals. Sham operation carried a 10% mortality.

The positioning of the ligature surrounding the left coronary artery influenced in a different manner the shape of the vessel and the degree of opening of the lumen. The effects of partial coronary ligation on the configuration and size of the arterial luminal diameter were apparent histologically (Fig. 2). At this level of resolution, amorphous material corresponding to the thread could be identified in the proximity of the vessel wall in association with an inflammatory reaction. The empty spaces surrounding the constricted vessels are a consequence of the displacement of the suture during sectioning. On the other hand, they provide an indirect indication of the location of the thread. In comparison with sham-operated controls, CAN produced an average 53% ($P < 0.001$) decrease in coronary diameter, which resulted in a 76% ($P < 0.001$) reduction in luminal cross-sectional area (Fig. 3). In summary, the methodology employed induced severe coronary artery stenosis.

Ventricular function. Hemodynamic measurements were collected from 16 sham-operated and 12 CAN mice. These parameters were obtained with a Millar catheter designed for the mouse heart that has a volume of 1 mm^3 (diameter = 0.71 mm; length = 2.54 mm). As described in *Ventricular size and shape*, the

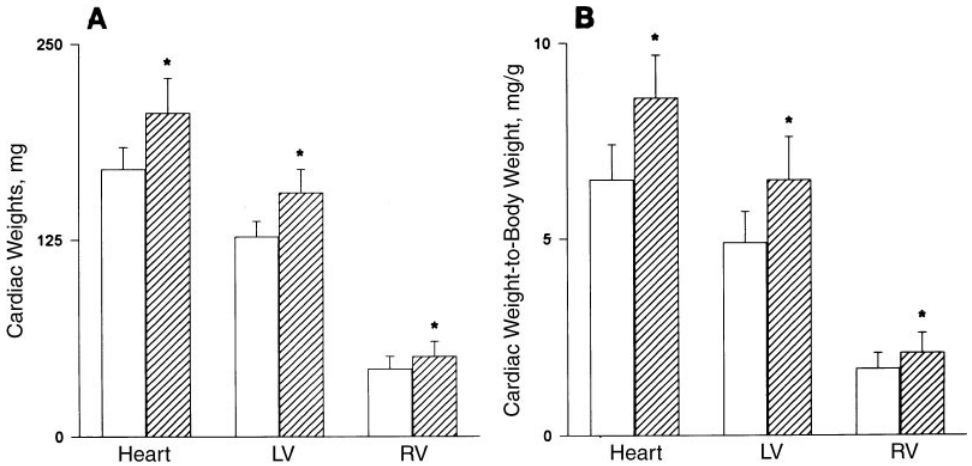

Fig. 1. Effects of coronary artery narrowing (CAN) on weight of the heart, left ventricle (LV), and right ventricle (RV) (*A*) and on ratios of heart, LV, and RV weight to body weight (*B*). Results are presented as means ± SD. *Statistically significant difference, $P < 0.05$. Open bars, sham-operated (SO) animals ($n = 16$); hatched bars, CAN mice ($n = 18$).

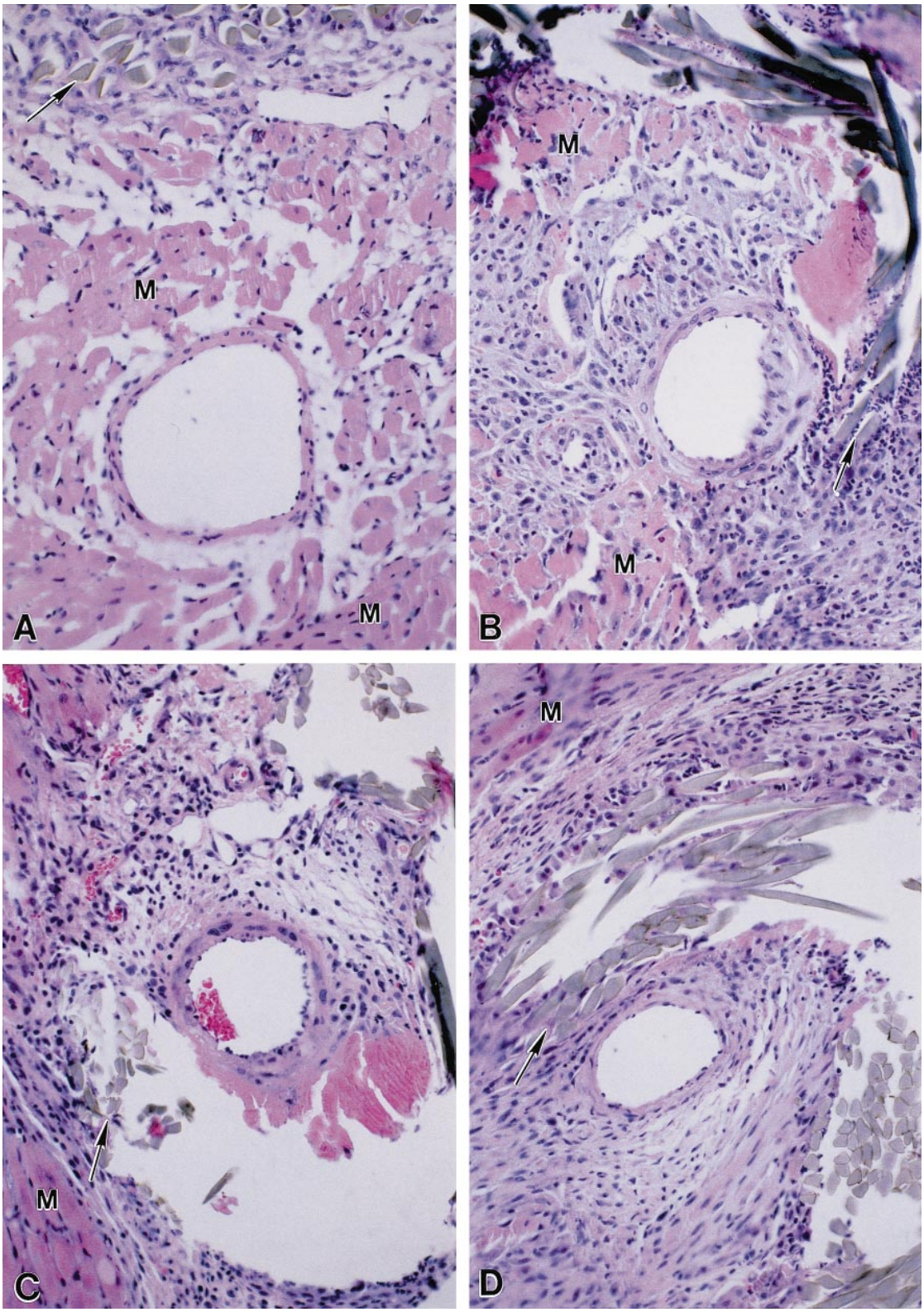

Fig. 2. Light micrographs of paraffin-embedded segments of left coronary artery near its origin obtained from a mouse in which constriction was minimal (*A*) and from 3 other animals with marked reductions in the vessel lumen (*B*, *C*, *D*). *A*, *B*, *C*, and *D* show percent reductions in luminal diameter of nearly 15, 40, 45, and 50%. A subacute inflammatory process is visible in the proximity of the coronary artery lumen. Empty space in *C* and *D* reflects location of suture that became detached during sectioning. Arrows correspond to positioning of parts of the suture closely adjacent to vessel wall. M, myocardium. Hematoxylin and eosin staining. *A*, *B*, *C*, *D*, ×220.

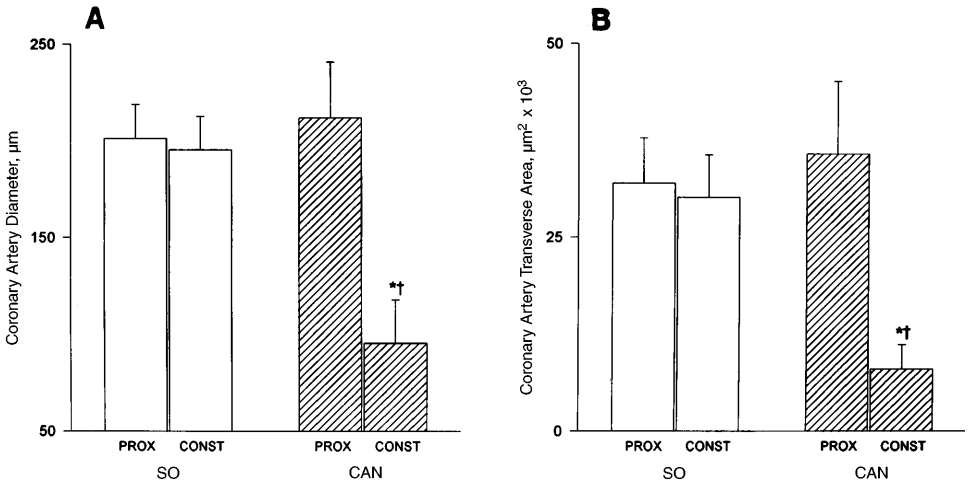

Fig. 3. Effects of CAN on diameter (*A*) and transverse area (*B*) of vessel lumen in region proximal to constriction (Prox) and at the level of constriction (Const). Results are presented as means ± SD. *Statistically significant difference from corresponding proximal segment, $P < 0.05$. †Statistically significant difference from corresponding region in SO mice, $P < 0.05$. SO, $n = 16$; CAN, $n = 18$.

volume of the left ventricular chamber varied from an average of 60 mm^3 in controls to 90 mm^3 in CAN mice. The evaluation of ventricular function in the closed chest preparation was associated with a 10% mortality in control animals and with a 30% rate of death in mice with CAN. Coronary artery stenosis at 7 days was characterized by the lack of changes in heart rate, from a control value of 467 ± 29 to a value of 486 ± 20 beats/min. In contrast, systolic blood pressure decreased 14% ($P < 0.005$), from 109 ± 12 to 94 ± 8 mmHg, and diastolic blood pressure decreased 9% ($P < 0.05$), from 78 ± 8 to 71 ± 9 mmHg. Mean blood pressure was reduced by 11% ($P < 0.01$), from 88 ± 9 to 78 ± 8 mmHg.

Figure 4 illustrates that alterations in left ventricular end-diastolic pressure (LVEDP), left ventricular systolic pressure (LVSP), and left ventricular + and −d*P*/d*t* occurred as a result of CAN. LVEDP increased 100% ($P < 0.001$) and LVSP decreased 15% ($P < 0.001$), provoking a 25% ($P < 0.001$) reduction in left ventricular developed pressure (LVDP), from 101 ± 13 to 76 ± 10 mmHg. Moreover, a 21 ($P < 0.001$) and an 11% ($P < 0.05$) decrease in left ventricular +d*P*/d*t* and −d*P*/d*t* was observed after coronary artery stenosis. In the 12 experimental animals, an attempt was made to determine whether a correlation existed between each hemodynamic parameter and the degree of CAN. Measurements of blood pressure and ventricular performance, including systolic, diastolic and mean arterial blood pressures, LVEDP, LVSP, LVDP, and + and −d*P*/d*t* did not correlate with the magnitude of CAN (data not shown). In summary, CAN was associated with left ventricular failure, but the severity of this alteration did not reflect the extent of constriction.

Ventricular size and shape. These measurements were obtained in 16 sham-operated and 18 CAN mice. Figure 5 depicts the changes in transverse chamber diameter and in the thickness of the free wall and septum as a consequence of coronary artery constriction. Seven days after CAN, cavitary diameter increased 20% ($P < 0.001$), whereas wall and septal thicknesses decreased 15 ($P < 0.001$) and 9% (not significant), respectively. These changes resulted in a significant reduction in the ratios of wall and septal thickness to chamber radius, −29 ($P < 0.001$) and −24% ($P < 0.001$). To establish whether these dimensional modifications in combination with the impairment in cardiac hemodynamics resulted in alterations in tension on the myocardium, diastolic stress was computed from the Laplace equation (sham-operated mice, $n = 16$; CAN mice, $n = 12$). This parameter increased 3.2-fold ($P < 0.001$) in the left ventricular free wall and 2.9-fold ($P < 0.001$) in the interventricular septum after CAN. Systolic wall stress could not be calculated because the changes in wall and septal thickness and chamber diameter during systolic contraction were not obtained. However, the reduction in LVSP was similar to the degree of thinning of the wall and of smaller magnitude than the expansion in cavitary radius, suggesting that an elevation in systolic stress may have occurred with coronary artery stenosis.

Additional characteristics relevant to the recognition of the magnitude of ventricular remodeling with coronary artery constriction are shown in Fig. 6. The major longitudinal axis of the ventricle increased 9% ($P < 0.005$). Moreover, the computation of chamber volume showed a 1.5-fold ($P < 0.001$) augmentation in ventricular cavitary size, which exceeded the 22% expansion in myocardial mass (Fig. 1*A*). These changes resulted in an 18% ($P < 0.01$) reduction in the ventricular mass-to-chamber volume ratio as a consequence of CAN for 7 days. Because transverse chamber diameter increased 2.2-fold more than the longitudinal diameter, coronary artery constriction was associated with a change in shape of the left ventricle toward a more spherical configuration. In summary, CAN enhanced diastolic wall stress, decreased the mass-to-chamber volume ratio, and altered cardiac geometry.

Myocardial damage. Light microscopic analysis of the left ventricular free wall showed that coronary artery constriction was accompanied by multiple sites of tissue injury that varied in nature, size, and distribution. These areas of damage were represented by foci of replacement fibrosis in various stages of evolution. At times, the collagen component prevailed on the cellular infiltrates (Fig. 7*A*), whereas, in other instances, inflammatory and connective tissue cells were particularly

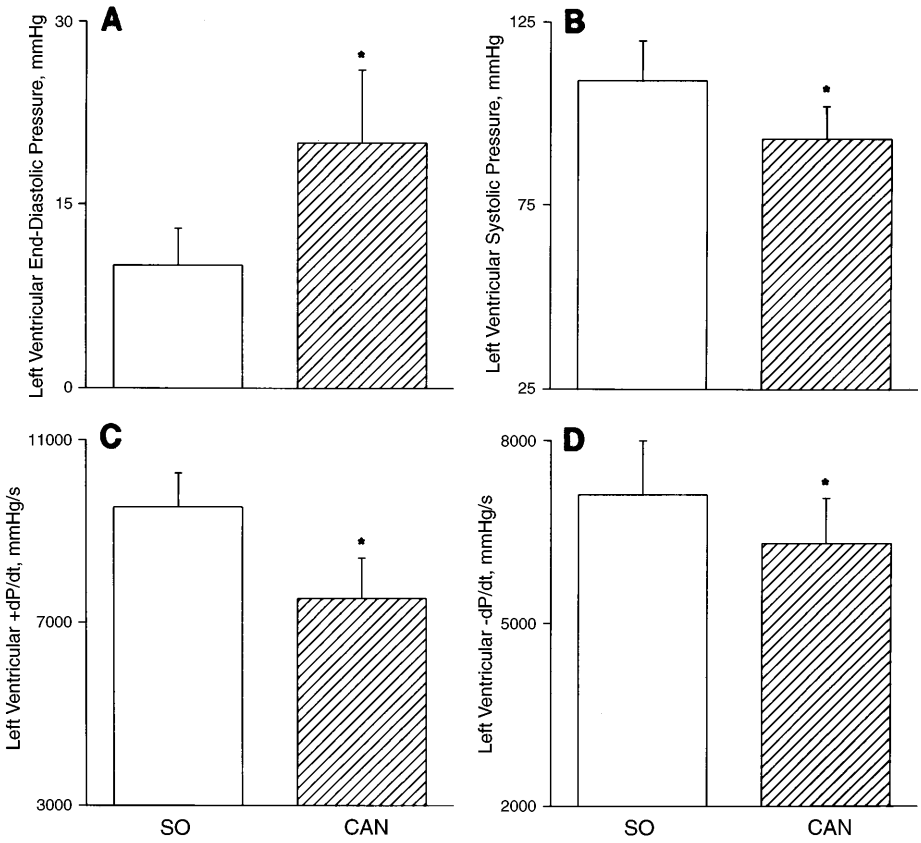

Fig. 4. Effects of CAN on left ventricular function. Results are presented as means ± SD. *Statistically significant difference, $P < 0.05$. SO, $n = 16$; CAN, $n = 12$.

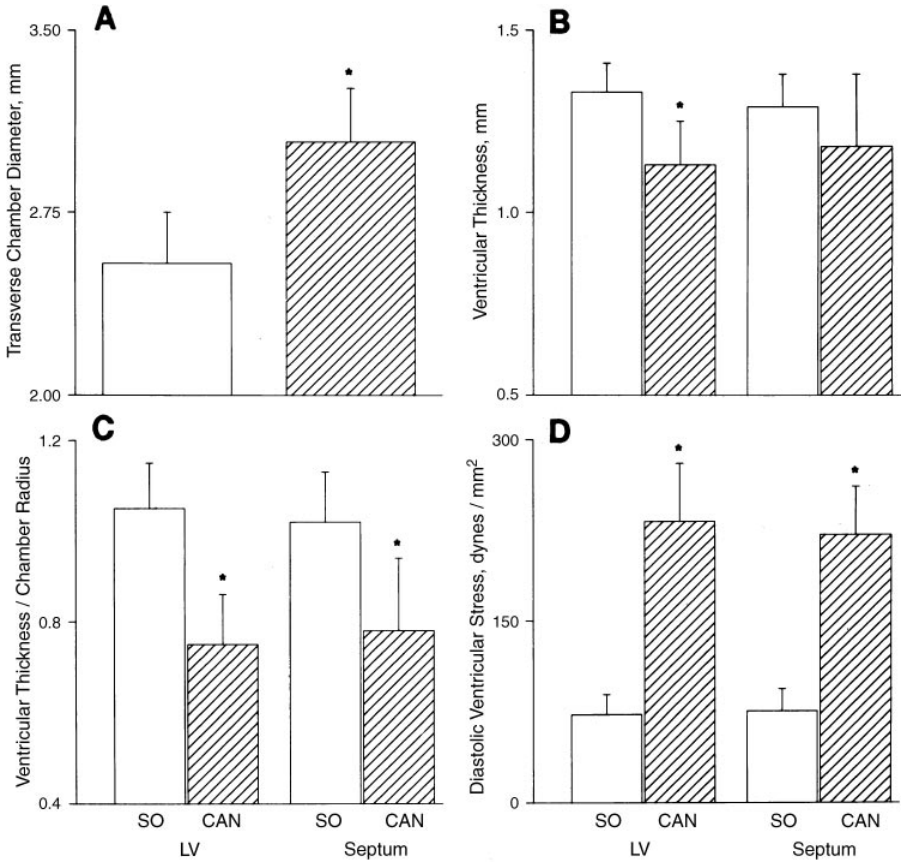

Fig. 5. Effects of CAN on dimensional properties of left ventricle and diastolic wall stress. Results are presented as means ± SD. *Statistically significant difference, $P < 0.05$. LV, left ventricular free wall; Septum, interventricular septum. *A*, *B*, and *C*: SO, $n = 16$; CAN, $n = 18$. *D*: SO, $n = 16$; CAN, $n = 12$.

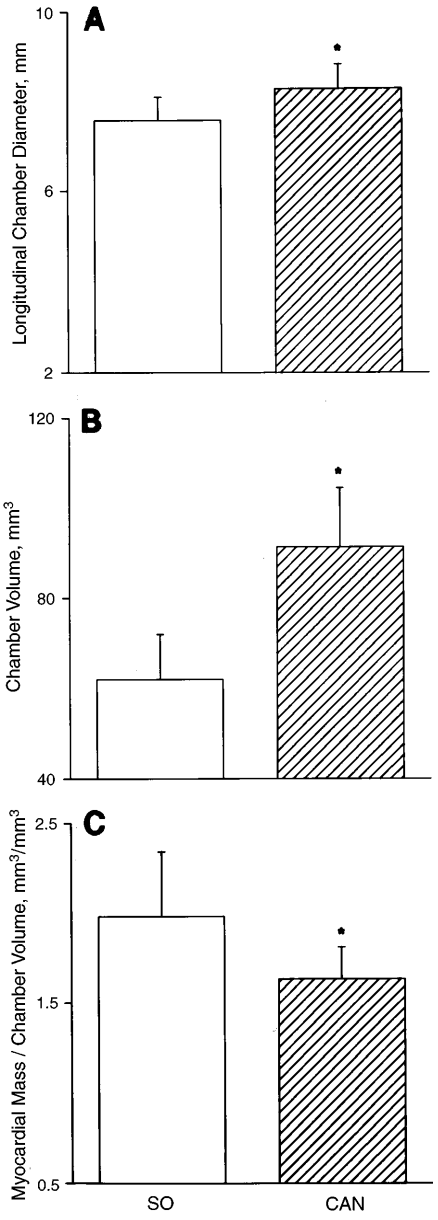

Fig. 6. Effects of CAN on major longitudinal cavitary axis (*A*), chamber volume (*B*), and myocardial mass-to-chamber volume ratio (*C*). Results are presented as means ± SD. *Statistically significant difference, $P < 0.05$. SO, $n = 16$; CAN, $n = 18$.

apparent (Fig. 7*B*). Contraction bands in myocytes (Fig. 7*C*) and disorganization of individual cells were also observed (Fig. 7*D*). These latter aspects of acute cell death were scattered across the ventricular wall but were more commonly detected in the endomyocardium. However, the discrete localization of these dying myocytes made their quantification very complex. Therefore, the evaluation of the numerical density, cross-sectional area, and volume percent of lesions in the myocardium after CAN was restricted to the foci of reparative fibrosis, independently from their structural characteristics. Nine sham-operated animals and 10 mice with CAN were included in this part of the study.

Figure 8*A* illustrates that CAN resulted in sites of replacement fibrosis in the myocardium that were of comparable dimension in the inner and outer layers of the left ventricular wall. However, with respect to sham-operated animals, these lesions were 10-fold ($P < 0.001$) and 15-fold ($P < 0.001$) larger in the epimyocardium and endomyocardium of mice subjected to coronary artery stenosis. Similarly, the number of damaged areas per square millimeter of tissue did not differ across the wall of CAN mice, but values 6.5-fold ($P < 0.001$) and 6.2-fold ($P < 0.001$) higher than in controls were found in the subendocardial and subepicardial region of the wall, respectively (Fig. 8*B*). Moreover, coronary artery constriction was associated with an 84-fold ($P < 0.001$) increase in the volume fraction of reparative fibrosis in the endomyocardium and 59-fold ($P < 0.001$) in the epimyocardium, resulting in an average 71-fold ($P < 0.001$) augmentation of this parameter across the entire wall (Fig. 8*C*). A correlation analysis between each of these morphological parameters and the extent of narrowing did not reach statistical significance. Additionally, the volume percent of damage in the interventricular septum was found to comprise 0.96 ± 0.27% of the myocardium. This evaluation was significantly lower than in the free wall ($P < 0.001$). When the left ventricle and septum were considered, the extent of injury involved 2.35 ± 0.65% of the tissue. In summary, CAN was characterized by acute and subacute myocardial damage of the left ventricle.

Number of myocyte nuclei in the ventricle and myocyte cell volume. The primary measurements that were used for the derivation of the numerical density of myocyte nuclei per unit volume of myocardium consisted of the determination of the number of myocyte nuclei per unit area of nondamaged tissue and of the evaluation of average nuclear length. The product of these average values combined with the aggregate volume of viable myocardium yielded the total number of myocyte nuclei in the ventricles (2). The results obtained in control and CAN mice are shown in Fig. 9*A*. In comparison with sham-operated animals, CAN mice exhibited a 15% ($P < 0.005$) loss in the total number of myocyte nuclei of the left ventricular wall and septum. These decreases in the total number of myocyte nuclei in the ventricle correspond to identical changes in myocyte number if the proportion between mononucleated and binucleated cells in the myocardium remains essentially constant (2).

Figure 9*B* shows the measurements of myocyte cell volume per nucleus obtained in the left ventricle of control and CAN mice. This parameter increased 38% ($P < 0.001$) after CAN. The increase in myocyte volume exceeded the expansion in left ventricular weight 22% ($P < 0.001$) because of the presence of tissue damage and cell loss. These factors resulted in an underestimation of the magnitude of reactive myocyte growth when measured at the organ weight level.

Correlation analysis. Table 1 illustrates the results of regression analysis correlating various functional and anatomic parameters with respect to the reduction in cross-sectional area of the coronary artery lumen. Measurements of ventricular performance, including LVEDP, LVSP, LVDP $+dP/dt$, and $-dP/dt$, did not

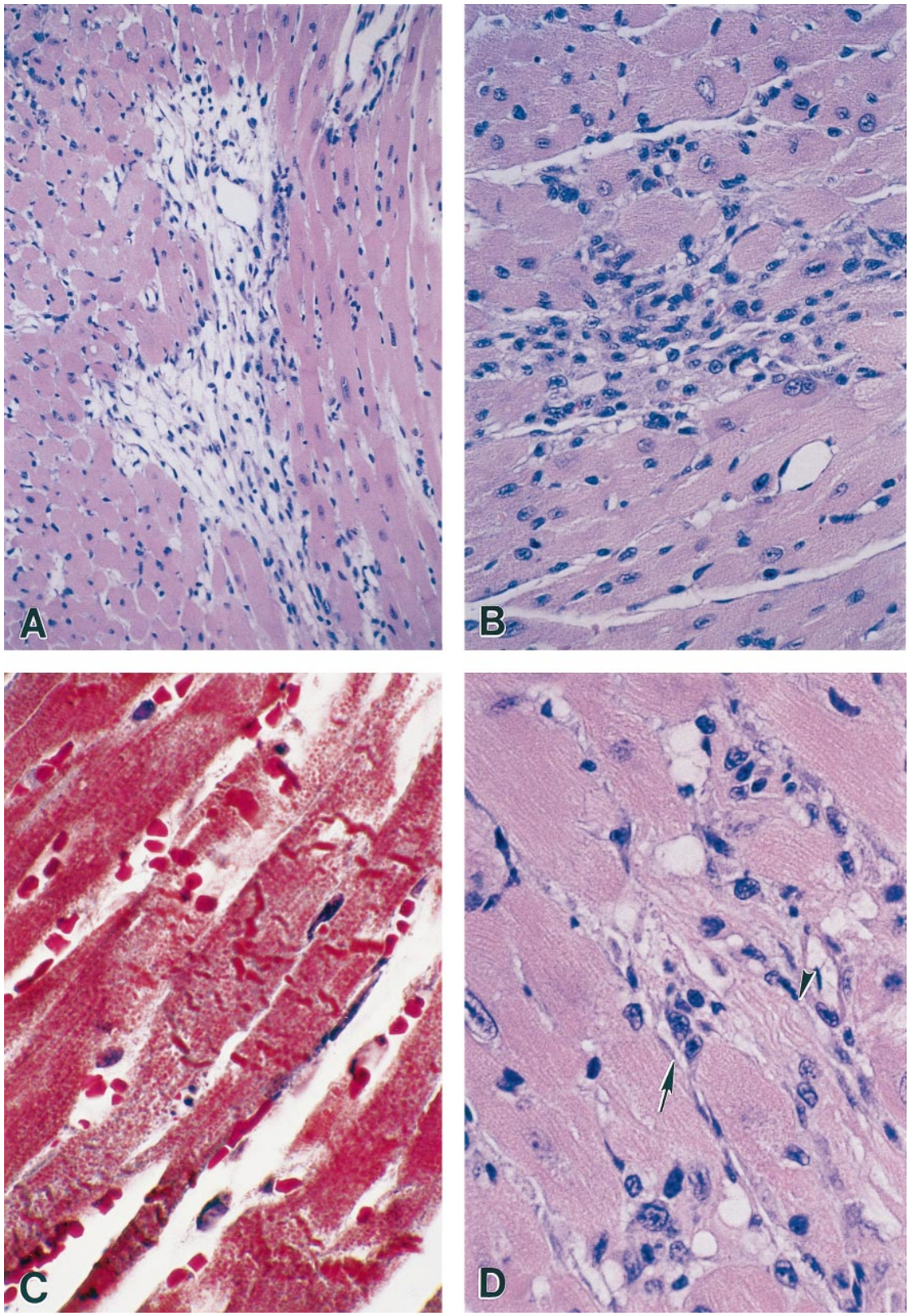

Fig. 7. Light micrographs of paraffin-embedded left ventricular myocardium illustrating an area of reparative fibrosis with little cellular infiltrates (*A*) and an area of myocyte loss with numerous inflammatory cells (*B*). Contraction bands in myocytes adjacent to normal cells are shown in *C*. *D* depicts a single myocyte loss (arrow) substituted by a small aggregate of inflammatory cells. Initial disorganization of the myocyte cytoplasm is evident in an adjacent cell (arrowhead). *A*, *B*, and *D*: hematoxylin and eosin staining; *C*: trichrome staining. *A*, ×225; *B*, ×350; *C* and *D*, ×750.

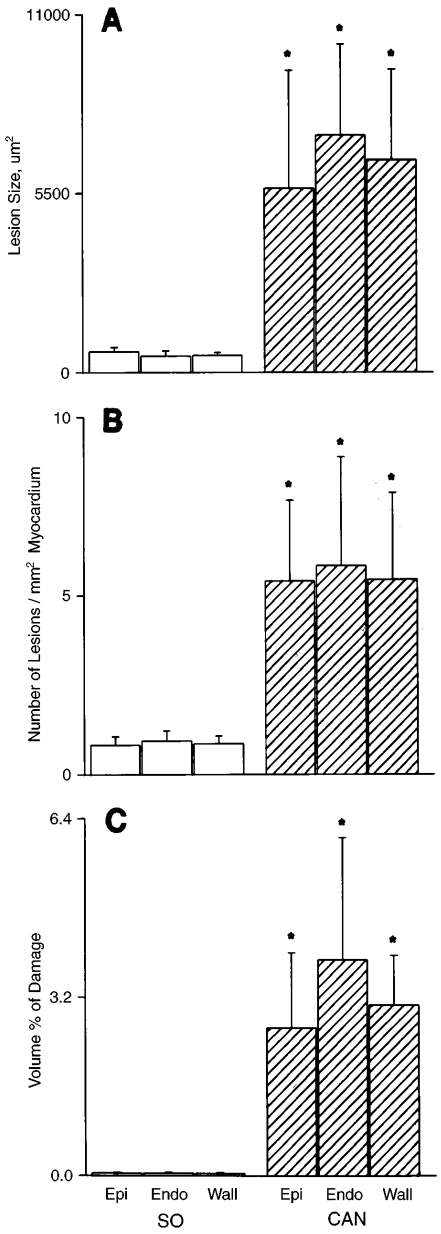

Fig. 8. Effects of CAN on the size (*A*), numerical density (*B*), and volume percent (*C*) of foci of replacement fibrosis in the epimyocardium (Epi), endomyocardium (Endo), and as an average across the wall (Wall). Results are presented as means ± SD. *Statistically significant difference, $P < 0.05$. SO, $n = 9$; CAN, $n = 10$.

correlate with the magnitude of CAN. Similarly, the typical aspects of ventricular remodeling, represented by left ventricular weight, chamber diameter, wall thickness, chamber volume, myocyte cell volume per nucleus, and total number of myocyte nuclei, were not correlated with the degree of coronary artery stenosis.

DISCUSSION

The results of the current study indicate that nonoccclusive constriction of the left main coronary artery was feasible in young adult mice, and this intervention provoked an average reduction in luminal diameter of 50%. Such a limitation in coronary perfusion for a period of 7 days was associated with alterations in cardiac function and myocardial loading, consisting of left ventricular failure and a marked elevation in diastolic wall stress. These hemodynamic abnormalities were coupled with extensive ventricular remodeling characterized by cavitary dilation and a decrease in wall thickness-to-chamber radius ratio. Moreover, cardiac hypertrophy occurred despite multiple foci of replacement fibrosis in various phases of healing and acute myocyte cell death in the ventricle. The combination of impaired pump performance, increased diastolic stress, myocyte loss, and decompensated eccentric hypertrophy after CAN in mice mimics the cardiomyopathic heart of ischemic origin in humans.

Coronary artery constriction and cardiac anatomy. Observations in animals and humans have demonstrated that ventricular dilation is a complicating event of acute and chronic cardiac dysfunction and failure of different etiology. This anatomic modification has been described in patients affected by ischemic heart disease (4, 7, 30), valvular defects (20), idiopathic dilated cardiomyopathy (25), and hypertensive hypertrophy when decompensation occurs (22). Similar results have been obtained in animal models attempting to reproduce these various pathological conditions (2, 23, 26). The current study provides additional documentation that coronary artery stenosis in mice was characterized by an increase in the longitudinal and transverse diameters of the left ventricle, resulting in a significant enlargement in chamber volume. Rats subjected to CAN also undergo comparable alterations in ventricular size shortly and long after the surgical intervention (2).

Two cellular mechanisms have been identified in the expansion of cavitary volume in the overloaded heart. The first one involves the structural rearrangement of the muscle compartment with side-to-side slippage of cells within the wall (1, 20). Muscle fiber slippage represents an early response to sudden increases in ventricular filling pressure and may account for most of mural thinning and ventricular dilation in the presence of acute diastolic Laplace overloading (1). This form of wall restructuring appears to require scattered myocyte cell death for mural translocation of cells to occur (11). The second aspect concerns changes in cell volume in response to tissue injury consisting of a predominant increase in myocyte length with respect to diameter (1, 20). Fiber elongation provides the structural template for a larger cavitary volume. A similar change may be obtained by the in-series addition of newly formed myocytes (20). However, these cellular modifications, reflecting myocyte hypertrophy and proliferation, are implicated in subacute and chronic chamber remodeling.

Results in the current investigation showed that myocardial damage and cardiac hypertrophy were detected in mice after CAN, suggesting that myocyte death and reactive growth processes may have been responsible for the alterations in cardiac anatomy. On the other hand, a cause-and-effect relationship between myocyte cell death and ventricular dilation remains to

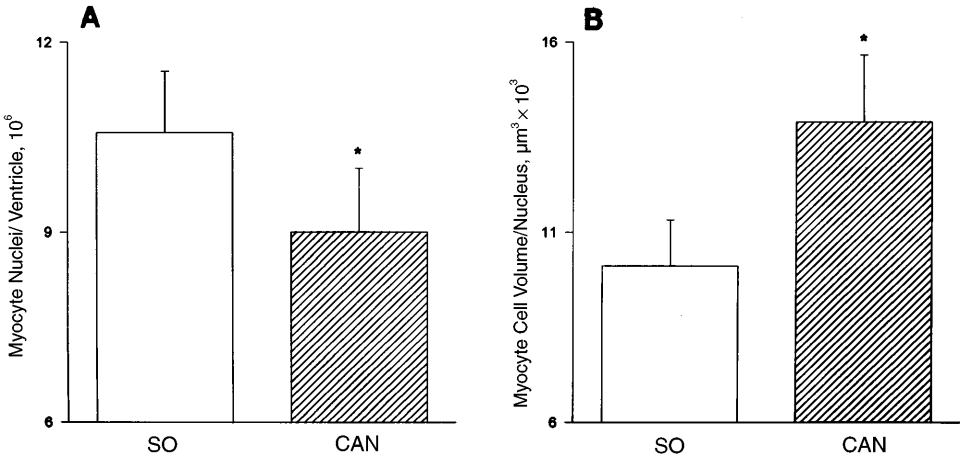

Fig. 9. Effects of CAN on total number of myocyte nuclei in left ventricle (*A*) and on myocyte cell volume per nucleus (*B*). Results are presented as means ± SD. *Statistically significant difference, $P < 0.05$. SO, $n = 9$, CAN, $n = 10$.

be demonstrated. This mouse model may offer the opportunity to answer this question because interventions involving the administration of growth factors, such as insulin-like growth factor 1 (IGF-1) may be applied to reduce tissue injury (24) and possibly the reorganization of the ventricular wall. Moreover and most importantly, transgenic mice overexpressing IGF-1 in myocytes have been developed (13), and CAN-induced myocyte cell death may be prevented or markedly reduced in these animals. If this is the case, the effects of impaired coronary perfusion on cardiac remodeling may be attenuated and new therapeutic strategies may be advanced in an attempt to interfere with the deleterious impact of chronic coronary atherosclerosis on the heart.

Coronary artery constriction and myocardial damage. The morphological characteristics of tissue and myocyte injury encountered in this investigation demonstrate that coronary artery stenosis was associated with ongoing acute myocyte cell death and discrete areas of reparative fibrosis. These temporarily distinct forms of cellular damage suggest that CAN may affect chronically the ventricular myocardium, paralleling the observations previously made in rats (9). The etiology of myocyte cell death in this model is difficult to ascertain. Measurements of coronary blood flow (CBF) were not obtained here, but maximal CBF decreases linearly with increasing degrees of coronary constriction in rats (9). Such a reduction in coronary flow reserve, in combination with the increase in oxygen consumption dictated by the elevation in ventricular wall stress, may create a local imbalance between oxygen supply and demand, leading to muscle cell death. The detection of contraction bands in myocytes raises the possibility that ischemia-reperfusion injury may have occurred as a result of transient spasm of the stenotic vessel (21). Additionally, platelet aggregation on the constricted segment (15) could have become detached, creating emboli in the distal portion of the coronary circulation and focal myocardial damage. Increased levels of circulating and tissue cathecolamines may have contributed to the development of sites of myocyte injury and reparative fibrosis (6). Of relevance, diastolic Laplace overloading and myocyte stretch may induce cell death (11). Because ischemia is associated with myocyte necrosis and apoptosis (18) and mechanical forces may activate the suicide program of myocytes (11), the question remains whether CAN is coupled with one or both types of cell death in mice.

A relevant characteristic of nonocclusive coronary artery constriction is the moderate degree of tissue injury that contrasts with the severity of impairment in cardiac performance. Such an association has been observed in various pathological conditions of the heart in humans (27) and in animal models (2, 9). Experimental results have indicated that a small continuous chronic loss of myocytes is critical in the initiation of ventricular dysfunction during aging (19) and genetically determined cardiomyopathy (13). Similarly, the extent of damage and fibrosis in markedly hypertrophied human hearts involves at most 10–15% of the myocardium (4, 20). However, the remaining healthy tissue is not capable of preserving ventricular hemodynamics despite a myocyte mass that is significantly higher than in normal hearts. This phenomenon has

Table 1. *Correlation analysis between coronary artery constriction and physiological and anatomic parameters*

	LVEDP	LVSP	LVDP	+dP/d*t*	−dP/d*t*	LVW	CD	WT	CV	MV	NN
n	12	12	12	12	12	12	12	12	12	10	10
r	0.0560	0.1230	−0.0945	−0.1020	−0.0250	−0.3310	0.3850	0.5200	−0.5134	0.1857	0.0597
P	0.813	0.656	0.726	0.712	0.833	0.305	0.225	0.075	0.092	0.542	0.804

Linear regression analysis comparing relationship between degree of coronary artery constriction, as a percentage of the total luminal cross-sectional area, and various parameters of cardiac function and structure. LVEDP, left ventricular end-diastolic pressure; LVSP, left ventricular systolic pressure; LVDP, left ventricular developed pressure; +dP/d*t*, peak rate of left ventricular pressure rise; −dP/d*t*, peak rate of left ventricular pressure decay; LVW, left ventricular weight; CD, chamber diameter; WT, wall thickness; CV, chamber volume; MV, myocyte volume per nucleus; NN, total number of myocyte nuclei.

been recognized in multivalvular defects (20), idiopathic dilated cardiomyopathy (25), long-term systemic hypertension in combination with aging (22), and in ischemic heart disease (4). Consistently, data in the current study indicate that ventricular failure was detected in mice after CAN in the presence of nearly 3% replacement fibrosis and 22% cardiac hypertrophy.

Myocyte loss, myocyte hypertrophy, and ventricular function. The severe impairment in ventricular performance in the presence of a 15% loss of myocytes and a 38% increase in volume of the remaining viable cells raises questions about the mechanism responsible for cardiac dysfunction after coronary stenosis. Reactive hypertrophy compensated for myocyte cell death, resulting in an increase in myocyte mass in the ventricle. However, the contractile behavior of the hypertrophied cells may be severely depressed in combination with alterations in cytosolic Ca^{2+} transients. Such a condition has been documented in the rat heart after coronary artery constriction (10). Defects in myocyte mechanics, extensive ventricular remodeling, and limitations in coronary perfusion may all contribute to the abnormalities in cardiac pump function observed in this model. Future studies will evaluate whether the isotonic and isometric properties of myocytes and their responsiveness to Ca^{2+} are impaired in mice with CAN.

The degree of coronary artery constriction failed to correlate with the changes in the physiological parameters of cardiac function and the extent of myocyte loss and cellular hypertrophy in the ventricle. This lack of association is difficult to explain but is consistent with observations in rats (2, 9) and humans (4, 7, 30, 31) with chronic narrowing of a major epicardial coronary artery. Pump performance and extent of vessel stenosis have been shown to be inversely related in large animals, only under acute experimental conditions (28); to the best of our knowledge, such a phenomenon remains to be demonstrated chronically in terms of magnitude of tissue damage, cell death, myocyte hypertrophy, and anatomic characteristics of ventricular remodeling. On the basis of previous results in rats (2, 9), the magnitude of myocardial hypertrophy in mice is expected to increase with the duration of coronary artery stenosis in the absence of an improvement in ventricular function. The possibility of interfering via molecular manipulations with reactive hypertrophy in the mouse model will allow a test of whether myocardial hypertrophy in ischemic cardiomyopathy constitutes a compensatory process or participates in the progression of ventricular dysfunction to terminal failure. This approach may involve the use of adenoviral vectors overexpressing inhibitors of myocyte growth such as IGF-1 binding proteins (5) or mitogen-activated protein phosphatases (16). Conversely, transgenic mice overexpressing IGF-1 may help to clarify if enhanced myocardial growth (24) may protect from the consequences of long-term ischemic damage, a possibility advanced experimentally in the postinfarcted heart (12) and in humans with severe cardiac failure (14).

Limitations of the study. Several limitations of the present study have to be acknowledged. Hemodynamic parameters were collected under anesthesia, and this procedure may have influenced these determinations in a different manner in control and CAN mice. The characterization of cardiac anatomy and the computation of diastolic wall stress after coronary artery stenosis required fixation of the left ventricle at the in vivo measured intracavitary end-diastolic pressure. This approach has provided an evaluation of ventricular dimensions and myocardial loading, closely mimicking the in vivo state, but has to be considered in the interpretation of the accumulated results. The surgical induction of coronary artery constriction in mice is complicated by the location of the vessel underneath the epicardial surface of the ventricular myocardium and the very small diameter of the lumen. These conditions affect the accuracy in the angle by which the ligature is positioned around the vessel and may influence the extent of the stenotic segment along the length of the vessel. The calculation of wall stress through the combination of in vivo measurements of ventricular pressure and postmortem determinations of mural thickness and chamber diameter is an oversimplification of the actual value in vivo. Although these limitations could not be avoided in the laboratory animal employed here, an attempt has been made to obtain information on the effects of impaired myocardial perfusion on the gross cardiac characteristics and stress distribution of the mouse heart.

The expert technical assistance of Maria Feliciano is greatly appreciated.

This work was supported by National Institute of Heart, Lung, and Blood Grants HL-38132, HL-39902, HL-43023, and HL-40561 and by Grant-in-Aid 950321 from the American Heart Association.

Address for reprint requests: P. Anversa, Dept. of Medicine, Vosburgh Pavilion, Rm. 302, New York Medical College, Valhalla, NY 10595.

Received 2 April 1997; accepted in final form 30 July 1997.

REFERENCES

1. **Anversa, P., G. Olivetti, L. G. Meggs, E. H. Sonnenblick, and J. M. Capasso.** Cardiac anatomy and ventricular loading after myocardial infarction. *Circulation* 87, *Suppl.* VII: VII-22–VII-27, 1993.
2. **Anversa, P., X. Zhang, P. Li, and J. M. Capasso.** Chronic coronary artery constriction leads to moderate myocyte loss and left ventricular dysfunction and failure in rats. *J. Clin. Invest.* 89: 618–629, 1992.
3. **Banai, S., M. T. Jaklitsch, M. Shou, D. F. Lazarous, M. Scheinowitz, S. Biro, S. E. Epstein, and E. F. Unger.** Angiogenic-induced enhancement of collateral blood flow to ischemic myocardium by vascular endothelial growth factor in dogs. *Circulation* 89: 2183–2189, 1994.
4. **Beltrami, C. A., N. Finato, M. Rocco, G. A. Feruglio, C. Puricelli, E. Cigola, F. Quaini, E. H. Sonnenblick, G. Olivetti, and P. Anversa.** Structural basis of end-stage failure in ischemic cardiomyopathy in humans. *Circulation* 89: 151–163, 1994.
5. **Benedict, M. R., M. J. Lu, J. R. Florini, J. Woo, and R. A. Richman.** The differential regulation of insulin-like growth factor (IGF) binding proteins by IGF-1 during the life span of the rat. *J. Gerontol. A Biol. Sci. Med. Sci.* 49: 215–223, 1994.
6. **Benjamin, I. J., E. Jalil, L. B. Tan, K. Cho, K. T. Weber, and W. A. Clark.** Isoproterenol-induced myocardial fibrosis in relation to myocyte necrosis. *Circ. Res.* 65: 657–670, 1989.
7. **Buja, L. M., and J. T. Willerson.** The role of coronary artery lesions in ischemic heart disease: insight from recent clinicopatho-

logic, coronary arteriographic, and experimental studies. *Hum. Pathol.* 18: 451–461, 1987.
8. **Buerke, M., T. Murohara, C. Skurk, C. Nuss, K. Tomaselli, and A. M. Lefer.** Cardioprotective effect of insulin-like growth factor 1 in myocardial ischemia followed by reperfusion. *Proc. Natl. Acad. Sci. USA* 92: 8031–8035, 1995.
9. **Capasso, J. M., P. Li, and P. Anversa.** Nonischemic origin of myocardial damage induced by short-term nonocclusive constriction of the coronary artery in rats. *Am. J. Physiol.* 260 (*Heart Circ. Physiol.* 29): H651–H661, 1991.
10. **Capasso, J. M., P. Li, and P. Anversa.** Cytosolic calcium transients in myocytes isolated from rats with ischemic heart failure. *Am. J. Physiol.* 265 (*Heart Circ. Physiol.* 34): H1953–H1964, 1993.
11. **Cheng, W., B. Li, J. Kajstura, P. Li, M. S. Wolin, E. H. Sonnenblick, T. H. Hintze, G. Olivetti, and P. Anversa.** Stretch-induced programmed myocyte cell death. *J. Clin. Invest.* 96: 2247–2259, 1995.
12. **Duerr, R. L., S. Huang, H. R. Miraliakbar, R. Clark, K. R. Chien, and J. Ross, Jr.** Insulin-like growth factor-1 enhances ventricular hypertrophy and function during the onset of experimental cardiac failure. *J. Clin. Invest.* 95: 619–627, 1995.
13. **Factor, S. M., T. Minase, S. Cho, R. Dominitz, and E. H. Sonnenblick.** Microvascular spasm in the cardiomyopathic Syrian hamster: a preventable cause of focal myocardial necrosis. *Circulation* 66: 342–354, 1982.
14. **Fazio, S., D. Sabatini, B. Capaldo, C. Vigorito, A. Giordano, R. Guida, F. Pardo, B. Biondi, and L. Saccà.** A preliminary study of growth hormone in the treatment of dilated cardiomyopathy. *N. Engl. J. Med.* 334: 809–814, 1996.
15. **Folts, J. D., K. Gallagher, and G. C. Rowe.** Blood flow reductions in stenosed canine coronary arteries: vasospasm or platelet aggregation. *Circulation* 65: 248–255, 1982.
16. **Hunter, T.** Protein kinases and phosphatases: the yin and yang of protein phosphorylation and signaling. *Cell* 80: 225–236, 1995.
17. **Kadambi, V. J., S. Ponniah, J. M. Harrer, B. D. Hoit, G. W. Dorn II, R. A. Walsh, and E. G. Kranias.** Cardiac-specific overexpression of phospholamban alters calcium kinetics and resultant cardiomyocyte mechanics in transgenic mice. *J. Clin. Invest.* 97: 533–539, 1996.
18. **Kajstura, J., W. Cheng, K. Reiss, W. A. Clark, E. H. Sonnenblick, S. Krajewski, J. C. Reed, G. Olivetti, and P. Anversa.** Apoptotic and necrotic myocyte cell deaths are independent contributing variables of infarct size in rats. *Lab. Invest.* 74: 86–107, 1996.
19. **Kajstura, J., W. Cheng, R. Sarangarajan, P. Li, B. Li, J. A. Nitahara, S. Chapnick, K. Reiss, G. Olivetti, and P. Anversa.** Necrotic and apoptotic myocyte cell death in the aging heart of Fischer 344 rats. *Am. J. Physiol.* 271 (*Heart Circ. Physiol.* 40): H1215–H1228, 1996.
20. **Linzbach, A. J.** Heart failure from the point of view of quantitative anatomy. *Am. J. Cardiol.* 5: 370–382, 1960.
21. **Maseri, A., and S. Chierchia.** Coronary artery spasm: demonstration, definition, diagnosis and consequences. *Prog. Cardiovasc. Dis.* 25: 169–192, 1982.
22. **Olivetti, G., M. Melissari, T. Balbi, F. Quaini, E. H. Sonnenblick, and P. Anversa.** Myocyte nuclear and possible cellular hyperplasia contribute to ventricular remodeling in the hypertrophic senescent heart in humans. *J. Am. Coll. Cardiol.* 24: 140–149, 1994.
23. **Pfeffer, M. A., and E. Braunwald.** Ventricular remodeling after myocardial infarction. *Circulation* 81: 1161–1172, 1990.
24. **Reiss, K., W. Cheng, A. Ferber, J. Kajstura, P. Li, B. Li, G. Olivetti, C. J. Homcy, R. Baserga, and P. Anversa.** Overexpression of insulin-like growth factor-1 in the heart is coupled with myocyte proliferation in transgenic mice. *Proc. Natl. Acad. Sci. USA* 93: 8630–8635, 1996.
25. **Roberts, W. C., R. J. Siegel, and B. M. McManus.** Idiopathic dilated cardiomyopathy: analysis of 152 necropsy patients. *Am. J. Cardiol.* 60: 1340–1355, 1987.
26. **Shannon, R. P., K. Komamura, B. S. Stambler, M. Bigaud, T. Manders, and S. F. Vatner.** Alterations in myocardial contractility in conscious dogs with dilated cardiomyopathy. *Am. J. Physiol.* 260 (*Heart Circ. Physiol.* 29): H1903–H1911, 1991.
27. **Schuster, E. H., and B. H. Bulkley.** Ischemic cardiomyopathy: a clinicopathologic study of fourteen patients. *Am. Heart J.* 100: 506–512, 1980.
28. **Vatner, S. F.** Correlation between acute reduction in myocardial blood flow and function in conscious dogs. *Circ. Res.* 47: 201–207, 1980.
29. **Veis, D. J., C. M. Sorenson, J. R. Shutter, and S. J. Korsmeyer.** Bcl-2-deficient mice demonstrate fulminant lymphoid apoptosis, polycystic kidneys, and hypopigmented hair. *Cell* 75: 229–240, 1993.
30. **Warnes, C. A., and W. C. Roberts.** Sudden coronary death: relation of amount and distribution of coronary narrowing at necropsy to previous symptoms of myocardial ischemia, left ventricular scarring and heart weight. *Am. J. Cardiol.* 54: 65–73, 1984.
31. **White, C. W., C. B. Wright, D. B. Doty, L. F. Hiratza, C. L. Eastham, D. G. Harrison, and M. L. Marcus.** Does the visual interpretation of the coronary arteriogram predict physiological significance of a coronary stenosis? *N. Engl. J. Med.* 310: 819–824, 1984.
32. **Wyman, R. M., E. R. Fahri, O. H. L. Bing, R. G. Johnson, R. M. Weintraub, and W. Grossman.** Comparative effects of hypoxia and ischemia in the isolated, blood-perfused dog heart: evaluation of left ventricular diastolic chamber distensibility and wall thickness. *Circ. Res.* 64: 121–128, 1989.